Journal of
Polymer Materials

Tech Science Press

http://doi.org/10.32604/jpm.2026.086582

ARTICLE

Synthesis of a Novel Hydrophobic Associating Polymer Stabilizer and Its Mechanism in Enhancing Viscosity Retention and Oil Recovery

Yong Qi[1], Jie Cao[2,*], Wanfa Liu[3] and Shiyuan Liu[4]

[1]College of Chemical Engineering, Sichuan University of Science & Engineering, Zigong, China
[2]School of Materials and Environmental Engineering, Chengdu Technological University, Chengdu, China
[3]The Second Oil Extraction Plant, Changqing Oilfield Branch, Qingyang, China
[4]The 12th Oil Extraction Plant, Changqing Oilfield Branch, Heshui, China
*Corresponding Author: Jie Cao. Email: caojie8488@163.com

Received: 02 June 2026; Accepted: 17 July 2026; Published: 24 September 2026

ABSTRACT: The viscosity of polymer solutions often decreases significantly due to shear degradation in near-wellbore zones and chemical/aging degradation during long-term transport, which seriously compromises the efficiency of polymer flooding. In this study, a hydrophobic monomer, hexadecyl dimethyl-5-enhexyl ammonium bromide (HAB), was synthesized. Subsequently, a novel viscosity stabilizer (LC12) was prepared via micellar polymerization of acrylamide and HAB using sodium dodecyl sulfate (SDS) as a solubilizer. The effect of this stabilizer on a hydrophobic associating polymer (AP-P4) was evaluated. Experimental results revealed that the addition of LC12 accelerated the dissolution rate of the polymer concentrate and significantly improved the viscoelasticity of the solution before and after degradation. Mechanistically, LC12 facilitates the formation of robust hydrophobic aggregates, shifting the retention mechanism from adsorption to mechanical trapping. Consequently, the shear viscosity retention of the AP-P4 solution increased by 28.4%, and the incremental oil recovery margin was improved by 4.49 percentage points after aging.

KEYWORDS: Enhanced Oil Recovery (EOR); polymer flooding; viscosity reduction; viscosity stabilizer

1 Introduction

As conventional hydrocarbon reserves mature, chemical enhanced oil recovery (CEOR) has emerged as a critical strategy to sustain global energy production [1]. Polymer flooding, in particular, is extensively deployed to optimize the mobility ratio and improve macroscopic sweep efficiency [2,3]. However, traditional partially hydrolyzed polyacrylamide (HPAM) suffers from severe viscosity loss due to high-shear degradation in near-wellbore regions and thermo-oxidative breakdown during extended transport in harsh [4], high-temperature, and high-salinity (HTHS) reservoirs [5,6]. To overcome these limitations, hydrophobically associating polymers (HAPs) have been developed [7,8]. These macromolecules form reversible, three-dimensional supramolecular networks via intermolecular hydrophobic interactions, exhibiting superior shear resistance and thermal stability compared to conventional HPAM [9]. Despite these advantages, HAPs still encounter critical bottlenecks in field applications [10–14], including slow dissolution kinetics and the progressive dissociation of hydrophobic clusters under prolonged exposure to severe reservoir conditions [15,16].

Conventionally, small-molecule stabilizers such as oxygen scavengers and chelating agents have been introduced to mitigate this degradation [17]. However, these traditional additives merely alter the local chemical environment to delay oxidative chain scission [18,19]. They fail to reinforce the physical integrity of the supramolecular network [20,21]. Consequently, their macroscopic performance is often limited, typically yielding only marginal improvements in viscosity retention or enhancing incremental oil recovery by a mere 1% to 2% [22]. This highlights a pressing necessity for the development of advanced polymeric stabilizers that can intrinsically fortify the network structure rather than simply scavenging reactive species. Recent advances emphasize the importance of microscopic displacement processes and transport behaviors in porous media [23,24]. As highlighted in a recent comprehensive review by Fu et al. [25], retention mechanisms and confined interfacial transport behaviors profoundly govern EOR efficiency [26–28]. Building upon these transport concepts, it becomes evident that an ideal stabilizer must not only inhibit chemical degradation but also mechanically strengthen the supramolecular architecture to optimize migration and retention behaviors in confined pore spaces.

To bridge this research gap, we designed and synthesized a novel polymeric viscosity stabilizer, LC12, via the micellar free-radical polymerization of acrylamide (AM) and a specifically tailored hydrophobic monomer, hexadecyl dimethyl-5-enhexyl ammonium bromide (HAB), utilizing sodium dodecyl sulfate (SDS) as a solubilizer. Unlike traditional small-molecule agents, LC12 functions as a structural reinforcer for the HAP matrix (AP-P4). We propose that LC12 operates through a "nucleation and bridging" mechanism, where its strongly hydrophobic segments aggregate with the hydrophobic domains of the polymer chains to form highly robust dynamic networks. This study systematically evaluates the synergistic effects of the LC12/AP-P4 system on dissolution, shear resistance, and long-term aging stability. Furthermore, we investigate how this structural reinforcement alters the fundamental retention mechanism from static surface adsorption to dynamic mechanical trapping, thereby evaluating its profound impact on mobility control and incremental oil recovery in porous media.

2 Experimental Section

2.1 Materials

(1) Chemicals

Hexadecyl amine, 6-bromo-1-hexene, butanone, acrylamide (AM), sodium dodecyl sulfate (SDS), potassium persulfate, deionized water, and nitrogen were the chemicals used in the experiments, and all were analytically pure and purchased from Chengdu Kelong Chemical Reagent Co. (Chengdu City, Sichuan Province, China).

The polymer used in this study was the hydrophobically associating polymer AP-P4, AP-P4 with solid content = 90%, insoluble content = 0.154%, degree of hydrolysis = 18.1%, molar fraction of hydrophobic groups of 2–5% and molecular weight = 13×10^6 and was purchased from Sichuan Guangya Polymer Chemical Co., Ltd. (Chengdu City, Sichuan Province, China).

The water used for the polymer solution preparation and repulsion experiments was simulated formation water with a mineralization of 9374.13 mg/L, and ionic composition is shown in Table 1.

Table 1: Ionic composition of the simulated formation water [29].

Ions	$Na^+ + K^+$	Ca^{2+}	Mg^{2+}	CO_3^{2-}	HCO_3^-	SO_4^{2-}	Cl^-	TDS
Concentration (mg/L)	3091.96	276.17	158.68	14.21	311.48	85.29	5436.34	9374.13

The crude oil used in the oil flooding experiment was oilfield simulated oil, with a viscosity of 70 mPa·s (65°C).

(2) Equipment

Equipment included a reflux reactor, triangular flask, stirrer, strainers, Brookfield DV-III, thermostat, Waring stirrer, UV spectrophotometer, MARS III Harker Rheometer, ISCO pump, quartz Sand.

(3) Core samples

The cores used for the determination of the resistance factor (R_F) and residual resistance factor (R_{RF}) are artificial short cylindrical cores (1#~6#), the cores used for the determination of the Oil displacement efficiency are synthetic cores (7#~12#), and the specific parameters are shown in Table 2.

Table 2: Core parameters.

Core Number	Core Size (mm)	Permeability (mD)	Pore Volume (mL)	Porosity (%)
1#	φ24.64 × 68.28	2022	11.43	34.83
2#	φ24.73 × 68.18	2012	11.09	33.90
3#	φ24.71 × 68.62	2035	11.47	34.83
4#	φ24.63 × 68.44	2037	11.50	35.32
5#	φ24.64 × 68.84	2455	11.66	35.54
6#	φ24.62 × 68.47	2479	11.68	35.85
7#	45 × 45 × 300	2643	184.01	30.29
8#	45 × 45 × 300	2431	184.07	30.30
9#	45 × 45 × 300	1559	184.13	30.31
10#	45 × 45 × 300	1746	166.75	27.45
11#	45 × 45 × 300	2369	181.64	29.90
12#	45 × 45 × 300	1998	184.07	30.30

All experiments were performed in triplicate, and the results are presented as mean ± standard deviation.

2.2 Synthesis of Viscosity Stabilizer

(1) Synthesis of hydrophobic monomer

Hydrophobic monomers are the core of viscosity stabilizers. Hexadecyldimethyl-5-enhexyl ammonium bromide (HAB) was designed for synthesis, and the synthetic route is shown in Fig. 1.

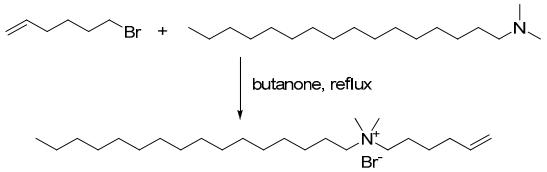

Figure 1: Synthetic route of HAB hydrophobic monomer.

A total of 24.15 g of hexadecyl amine and 17.94 g of 6-bromo-1-hexene were placed in a circular flask, and 22.72 g of butanone was added as a solvent for the reflux reaction to form the HAB hydrophobic monomer.

(2) Copolymer: Acrylamide/Hexadecyldimethyl-5-enhexyl ammonium bromide (AM-co-HAB)

The hydrophobically associating copolymer, AM-co-HAB (Fig. 2), was synthesized via micellar free-radical polymerization. Predetermined amounts of acrylamide (AM), hydrophobic monomer (HAB), and sodium dodecyl sulfate (SDS) were dissolved in deionized water and charged into a reactor (Table 3). It is important to note that SDS was employed solely as a surfactant to solubilize the hydrophobic HAB

monomer within the aqueous phase and form micelles, serving as the locus for polymerization, rather than acting as a comonomer. The reaction mixture was stirred and purged with nitrogen gas to eliminate dissolved oxygen. The reactor was then placed in a constant-temperature water bath maintained at 65–80°C. Once the temperature stabilized, potassium persulfate was added as an initiator, and the polymerization reaction proceeded under a continuous nitrogen atmosphere for 1.5–7 h.

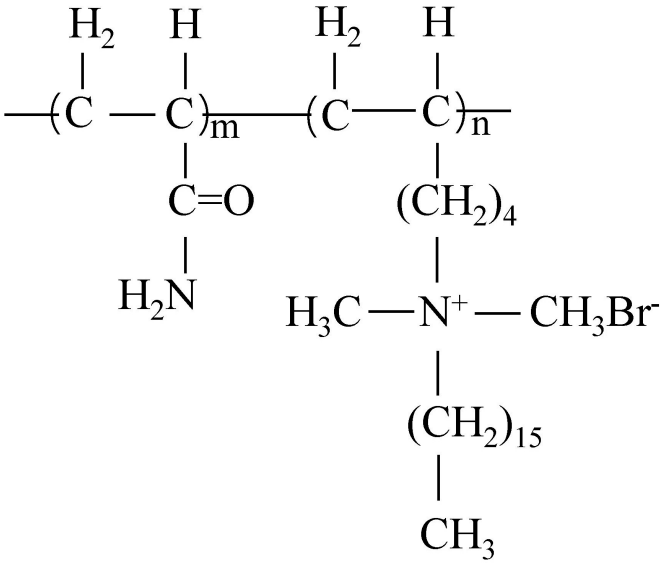

Figure 2: Structural formula of AM-co-HAB.

Table 3: Reaction conditions of AM-co-HAB copolymerization.

Copolymer Name	LC9	LC10	LC11	LC12
AM (g)	3.998	3.994	4.112	4.084
HAB (g)	0.499	0.511	0.510	0.982
SDS (g)	2.084	3.999	1.020	2.245
Potassium persulfate (g)	0.009	0.008	0.008	0.007
De-ionized water (mL)	50	65	57	70
Reaction time (h)	4	2	1.5	6
Temperature (°C)	80	75	70	65

The specific variations in the synthesis conditions listed in Table 3 directly dictate the microstructural architecture and sequence distribution (blockiness) of the resulting copolymers. In micellar free-radical polymerization, the feed ratio of the hydrophobic monomer (HAB) and the concentration of the surfactant (SDS) jointly govern the average number of hydrophobic monomers per micelle (micellar occupancy, N_H). For LC9 and LC10, the lower HAB feeding content results in a highly sparse distribution of hydrophobic groups along the hydrophilic polyacrylamide (PAM) backbone. These short, isolated hydrophobic segments predominantly participate in weak, scattered intramolecular associations, failing to establish an extensive network. For LC11, increasing the HAB content without a perfectly optimized surfactant-to-monomer ratio leads to broader composition heterogeneity. In contrast, LC12 is synthesized under an optimal balance (0.8% HAB and a 3.0 SDS/HAB ratio), which yields an ideal hydrophobic block length and optimal sequence frequency. This specific microstructural architecture maximizes its capacity to act as ‘association nuclei’, allowing LC12 to efficiently form robust intermolecular ‘bridges’ with the parent polymer (AP-P4) chains rather than collapsing into self-associations.

2.3 Screening Method for Viscosity Stabilizer

The four synthetic viscosity stabilizers were added to the AP-P4 solution at a concentration of 1750 mg/L, and the amount of stabilizer was 25 mg/L. The best viscosity stabilizer was determined by measuring the half-life of the viscosity reduction of the solution. The Viscosity half-decay time $t_{1/2}$ is the time corresponding to the reduction of the polymer solution viscosity value from the maximum value to half. The longer the half-life is, the better the viscosity stabilization effect, and the greater viscosity is, the stronger the viscosity increase effect.

2.4 The Effect of Viscosity Stabilizers on the Polymer Properties

(1) Influence on the polymer dissolution process

The viscosity stabilizer and the dry powder of hydrophobic polymer AP-P4 were added to the simulated formation water without considering the solid content of the hydrophobic polymer, so that the total concentration of viscosity stabilizer and polymer AP-P4 was 5000 mg/L, and the same concentration of polymer solution without viscosity stabilizer was also prepared as a control sample without the stabilizer for comparison.

Appropriate amounts of polymer solution were taken at polymer dissolution times of 20, 40, 70, 105, 135, and 165 min and passed through a filter at a pressure of 0.01 MPa to determine the amount of undissolved polymer AP-P4 at different preparation conditions and times.

(2) Shear stability

The polymer AP-P4 master batch prepared under different conditions at a concentration of 5000 mg/L was diluted to a concentration of 1750 mg/L and sheared for 20 s at a specific speed (Speed Setting 1, approx. 3500 rpm) in a Waring stirrer, and the viscosity retention of the polymer solution was measured before and after shearing.

(3) Ageing stability

The polymer solution with a concentration of 1750 mg/L was aged in a constant temperature chamber at 65°C for 120 d. The viscosity of the polymer solution was measured by taking samples at 1, 5, 11, 17, 24, 33, and 46 d, to evaluate the ageing performance.

(4) Static adsorption amount of polymer

First, a series of AP-P4 solutions with low concentrations of added and unadded stabilizer were prepared, and the absorbance of AP-P4 solutions with different concentrations after ageing for 0, 24, and 46 d was measured by UV spectrophotometer. The standard relationship curves between absorbance and concentration of polymer solutions were plotted, and the corresponding curve relationship equations were obtained by fitting. The polymer solution with a concentration of 1750 mg/L was transferred into glass vials containing 100 mesh quartz sand at a solid-liquid mass ratio of 1:10 and shaken periodically. After adsorption equilibrium was reached, the absorbance of the supernatant was measured using a UV spectrophotometer. The concentration was calculated based on the fitted standard curve relationship equation, and finally, the static adsorption amount was obtained by calculation.

(5) Rheological properties

The rheology and viscoelasticity of polymer solutions with a concentration of 1750 mg/L were determined at different shear rates after ageing times of 0, 24, and 46 d using a MARS III Harker Rheometer.

(6) R_F and R_{RF}

The polymer solution with a concentration of 1750 mg/L was subjected to cylindrical core flow experiments after ageing for 0, 24, and 46 d. The initial pressure P_0, water drive smooth pressure P_1, poly drive smooth pressure P_2, and post water drive smooth pressure P_3 were recorded, where the repulsion rate for the water drive, poly drive, and post water drive processes was 0.5 mL/min. R_F and R_{RF} were calculated according to Eqs. (1) and (2). The experimental flow chart is shown in Fig. 3.

$$R_F = \frac{P_2 - P_0}{P_1 - P_0} \tag{1}$$

$$R_{RF} = \frac{P_3 - P_0}{P_1 - P_0} \tag{2}$$

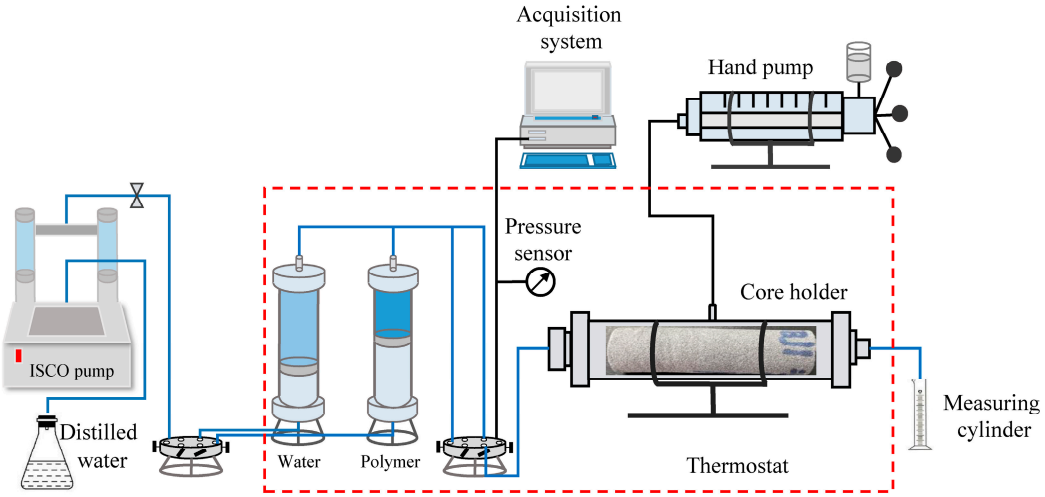

Figure 3: Flow chart of seepage characteristics determination.

(7) Oil flooding performance

The polymer solution with a concentration of 1750 mg/L was subjected to oil flooding experiments in square cores after ageing for 0, 24, and 46 d. First, the square core was evacuated and saturated with simulated formation water, and the pore volume was determined using the weighing method. After measuring the core water measurement permeability, oil saturation was performed. The oil used was a simulated oil with a viscosity of 70 mPa·s. The cores need to be aged for two weeks after oil saturation before the replacement experiments could be performed.

Oil flooding experiments were conducted in accordance with the experimental procedure, experimental data on time were recorded, and the water flooding recovery rate and polymer flooding recovery rate were calculated. The experimental flow chart is shown in Fig. 4.

3 Results and Discussion

3.1 Viscosity Stabilizer Selection

The results of the viscosity half-decay time of AP-P4 solution with different stabilizers added at a concentration of 1750 mg/L are shown in Table 4. The half-life of the polymer solution viscosity after adding LC9, LC10, and LC11 remained the same compared with the polymer solution without the viscosity

stabilizer, while the half-life of the polymer solution viscosity after adding LC12 reached more than twice that of the blank solution, which indicates that LC12 has a good viscosity stabilizing ability. At the same time, the addition of LC12 was accompanied by a certain viscosity increasing effect. Therefore, considering the viscosity stabilization effect and the cost of polymerization injection, LC12 was finally selected as the final viscosity stabilizer for the subsequent study.

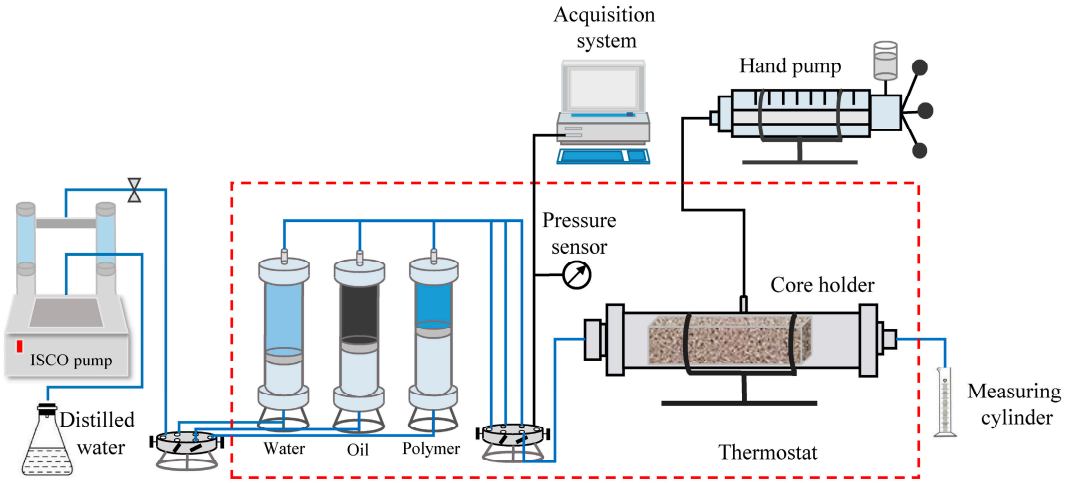

Figure 4: Flow chart of the oil flooding experiment.

Table 4: Viscosity half-decay time of AP-P4 solution before and after the addition of stabilizer.

Samples	AP-P4	AP-P4+LC9	AP-P4+LC10	AP-P4+LC11	AP-P4+LC12
$t_{1/2}$ (d)	29.1	27.2	29.2	29.8	55.8
$\eta_{1/2}$ (mPa·s)	13.5	19.5	22.0	21.5	24.0
$t/t_{(No.1)}$	1.00	0.94	1.00	1.02	1.91
$\eta/\eta_{(No.1)}$	1.00	1.44	1.63	1.59	1.78

After determining the viscosity stabilizer as LC12, the dosage of LC12 was optimized, and LC12 was added to the 1750 m/L solution of polymer AP-P4 at concentrations of 15, 20, 25, 30, and 50 mg/L, respectively, to study the viscosity half-decay time of the viscosity of the solution of polymer AP-P4 under the conditions of different concentrations of LC12, and the results are shown in Table 5. As can be seen in Table 5, when the concentration of LC12 is ≤25 mg/L, the viscosity half-decay time and the viscosity corresponding to the half-life of the polymer AP-P4 solution after the addition of LC increase with the increase in the concentration of LC12, but when the concentration of LC12 added is >25 mg/L, the viscosity half-decay time and the viscosity corresponding to the half-life change very little with increasing LC12 concentration. The optimum concentration of LC12 was chosen to be 25 mg/L by combining the cost and other factors.

Table 5: Viscosity half-decay time of AP-P4 solutions after addition of different concentrations of LC12.

The Concentration of LC12	0	15	20	25	30	50
$t_{1/2}$ (d)	29.1	30.4	37.9	55.8	56.5	57.2
$\eta_{1/2}$ (mPa·s)	13.5	13.4	15.4	24.0	23.1	22.7
$t/t_{(No.1)}$	1.00	1.04	1.30	1.91	1.94	1.96
$\eta/\eta_{(No.1)}$	1.00	0.99	1.14	1.78	1.71	1.68

The significant stabilization effect of trace amounts of LC12 (25 mg/L) on the AP-P4 system can be attributed to a 'nucleation and bridging' mechanism. Although the concentration of LC12 is low, its strongly hydrophobic HAB blocks act as association nuclei. These nuclei interact with the hydrophobic domains of the AP-P4 chains, creating a denser and more robust supramolecular network [30,31].

The observed decline in solution viscosity during the aging tests, particularly under laboratory semi-closed conditions at elevated temperatures, is primarily attributed to thermo-oxidative degradation. The synergistic effect of thermal energy and residual oxygen triggers the generation of free radicals, which subsequently initiate the oxidative scission of the polymer's carbon-carbon backbone. This chain scission process results in a significant reduction in molecular weight and the disintegration of the three-dimensional supramolecular network, leading to a loss in bulk viscosity. Notably, the incorporation of LC12 effectively mitigates this degradation. Mechanistically, the protective effect of LC12 is attributed to the reduced polymer chain mobility and accessibility, the restricted oxygen diffusion through the denser hydrophobic association network, and possibly the radical-scavenging capability of LC12 itself, rather than a simple physical barrier.

3.2 Evaluation of the Effect of the Viscosity Stabilizer on the Polymer Properties

(1) Influence on the polymer dissolution process

To comprehensively understand the macroscopic performance of the AP-P4/LC12 system, it is essential to establish a robust structure–property relationship. As recently elucidated by Deng et al. [32], the macroscopic viscoelasticity and stimulus-responsiveness of supramolecular assemblies are fundamentally governed by their underlying molecular architecture. In this study, the tailored molecular architecture of the LC12 stabilizer—specifically the incorporation of strongly hydrophobic hexadecyl dimethyl-5-enhexyl ammonium bromide (HAB) blocks—acts as a topological director. These hydrophobic domains serve as robust association nuclei that dynamically bridge the AP-P4 polymer chains. This distinct architectural design dictates the macroscopic properties across three critical dimensions: (1) Dissolution: At the initial hydration stage, the specific arrangement of the surfactant-monomer complexes temporarily shields intermolecular hydrophobic interactions, structurally preventing the formation of impermeable macroscopic aggregates (the "fish-eye" effect) and enabling rapid water penetration. (2) Rheology: Under dynamic shearing, the reversible physical cross-linking established by the HAB blocks facilitates a rapid disentanglement and re-entanglement equilibrium. This molecular-level structural flexibility translates macroscopically into elevated elastic (G′) and viscous (G′) moduli. (3) Stability: During long-term HTHS ageing, while the primary C-C backbone of AP-P4 may undergo partial thermo-oxidative scission, the dense supramolecular nodes formed by LC12 proactively confine the dissociated chain fragments. This architectural reinforcement preserves the physical integrity of the spatial network, thereby delivering the exceptional macroscopic viscosity retention observed in the ageing tests.

The variation in the residue content of the polymer AP-P4 dissolution process with time and the variation in the polymer solution viscosity with time after the addition of the viscosity stabilizer LC12 are shown in Fig. 5. It can be seen from the graph that the residue content of the blank AP-P4 solution remained at 100% until 80 min, after which it began to drop, reaching approximately 19% at 165 min. In contrast, the AP-P4 solution containing the LC12 stabilizer demonstrated rapid initial dissolution, with the residue content dropping to 87.5% at just 70 min and further decreasing to 22.0% at 180 min, indicating that the stabilizer significantly accelerates the disentanglement of the polymer chains.

Mechanistically, the inherently strong intermolecular hydrophobic associations of AP-P4 often cause the dry polymer powder to form an impermeable exterior gel layer ("fish-eye" effect) upon initial contact

with water, severely hindering further water penetration and chain disentanglement. The addition of LC12 fundamental alters this hydration kinetic. The sodium dodecyl sulfate (SDS) molecules and the tailored HAB hydrophobic domains within the LC12 system actively reduce the interfacial tension at the solid-liquid interface. More critically, the micellar structures selectively encapsulate and temporarily shield the exposed hydrophobic groups on the outer AP-P4 chains. This micellar shielding effect temporarily suppresses premature inter-chain hydrophobic aggregation at the water-powder boundary, preventing the formation of a dense, water-blocking shell. Consequently, free water molecules can rapidly penetrate the core of the polymer agglomerates, accelerating the swelling and subsequent hydrodynamic disentanglement of the polymer chains into a homogeneous macroscopic solution.

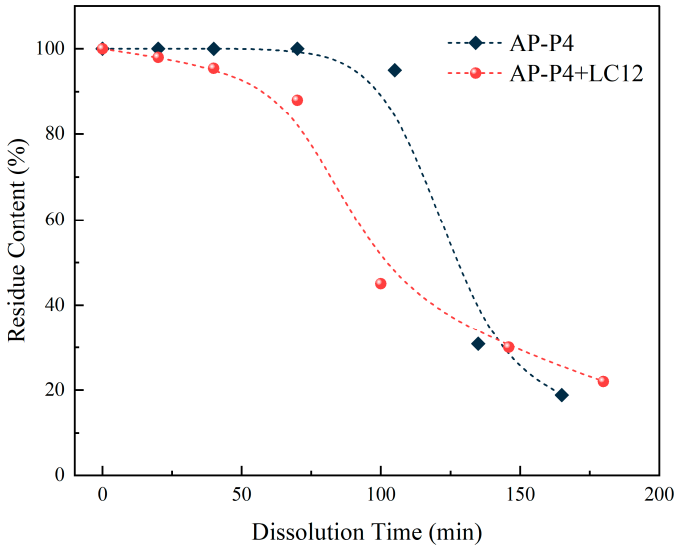

Figure 5: Variation in residue content with dissolution time.

(2) Shear stability

The polymer AP-P4 master batch with a concentration of 5000 mg/L was diluted to a concentration of 1750 mg/L and then sheared by a Waring stirrer, and the results of the solution viscosity before and after shearing are shown in Table 6.

Table 6: Retention of solution viscosity before and after shearing.

Samples	Viscosity (mPa·s)		Viscosity Retention (%)
	Before Shearing	After Shearing	
AP-P4	27.0	5.2	19.3%
AP-P4+LC12	48.0	22.9	47.7%

The viscosity values and viscosity retention before and after shear were higher for the system with the addition of LC12 than for the blank solution, indicating that the stabilizer was able to improve the shear resistance of the AP-P4 solution. This improvement is attributed to the reversible nature of the hydrophobic association network reinforced by LC12: the network temporarily disassembles under high shear to dissipate energy, then rapidly reassembles after passing through the high-shear zone, minimizing irreversible chain scission. In the reservoir, this means that a higher effective viscosity can be maintained as the solution enters the deep formation.

(3) Ageing stability

The effect of ageing time on the viscosity of the AP-P4 solution before and after the addition of the stabilizer is shown in Fig. 6. During the 46-day aging period, the viscosity of the blank AP-P4 solution decreased sharply, dropping to a final value of 7.8 mPa·s. However, the LC12 stabilized solution maintained a significantly higher overall viscosity throughout the test, retaining 18.7 mPa·s at 46 days, which is 2.4 times higher than that of the blank solution. This indicates that the viscosity stabilizer can effectively slow down the ageing degradation of the AP-P4 solution. This result is of particular significance for deep reservoirs with long transport distances. It ensures that the polymer solution maintains sufficient mobility control throughout the entire transport cycle, thereby preventing premature water breakthrough and maximizing the sweep efficiency of the entire reservoir.

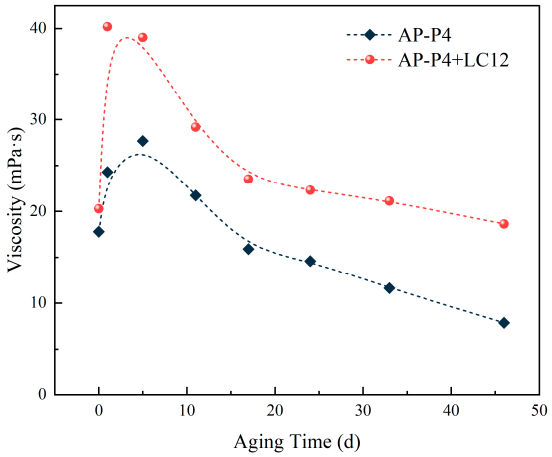

Figure 6: Influence of stabilizers on the viscosity of AP-P4 solution at different ageing times.

Finally, it is necessary to address the boundary conditions of the aging stability tests. In this study, the thermal ageing was intentionally performed under 'semi-closed' conditions without preliminary nitrogen bubbling or dissolved oxygen (DO) control. In actual deep oil reservoirs, the environment is intrinsically anaerobic (DO typically < 50 ppb). By contrast, our experimental setup allows the presence of ambient dissolved oxygen, which creates an accelerated thermo-oxidative degradation environment driven by oxygen-derived free radicals—essentially representing a 'worst-case scenario' for the polymer network.

The fact that the AP-P4/LC12 system still managed to deliver exceptional macroscopic viscosity retention under such un-deoxygenated, oxidative stress highlights its remarkable chemical and structural robustness. For field applications, while standard surface deoxygenation processes (e.g., nitrogen stripping) are always recommended to eliminate bulk oxygen, LC12 functions as an indispensable secondary defense line. It provides an engineering safety margin capable of safeguarding the supramolecular network against localized oxygen ingress caused by accidental wellhead leaks or oxygen-rich water handling, thereby ensuring prolonged mobility control in deep formations.

(4) Static adsorption

The absorbance versus concentration curves of the polymer solutions with or without an stabilizer before and after ageing at low concentrations were measured by UV spectrophotometer and are shown in Fig. 7. The linear relationship between absorbance and concentration of the polymer solution was obtained by fitting the measured experimental results, which are shown in Table 7.

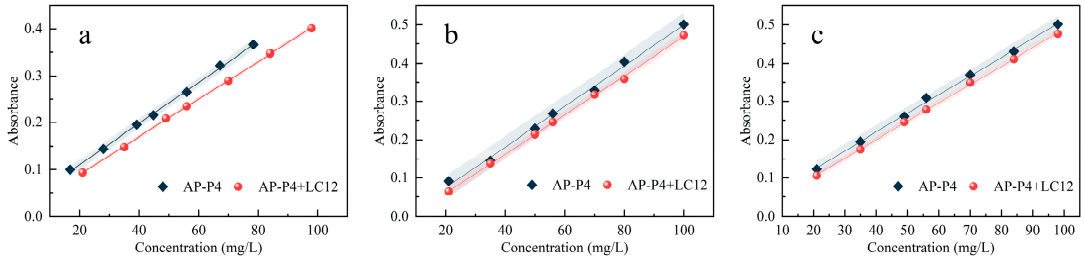

Figure 7: Static adsorption standard curve ((**a**): ageing 0 d; (**b**): ageing 24 d; (**c**): ageing 46 d).

Table 7: Standard curve fitting parameters.

Samples	Aging Time (d)	Fitted Curves y = a + bx	R^2	Curve No.
AP-P4	0	y = 0.023 + 0.00438x	0.99855	I
AP-P4+LC12		y = 0.00927 + 0.00402x	0.99977	II
AP-P4	24	y = 0.03016 + 0.00531x	0.99624	III
AP-P4+LC12		y = 0.04454 + 0.00517x	0.99974	IV
AP-P4	46	y = 0.02431 + 0.00489x	0.99780	V
AP-P4+LC12		y = 0.00735 + 0.00481x	0.99949	VI

The concentration of the polymer solution after adsorption was obtained by substituting the fitted standard curve equation according to the absorbance of the polymer solution with a concentration gradient formed after dilution, and the static adsorption amount was calculated after taking the average value of the concentration. The experimental data and calculated results are shown in Table 8.

Table 8: Calculation results of static adsorption of polymer solution.

Aging Time (d)	0		24		46	
Samples	**AP-P4**	**AP-P4+LC12**	**AP-P4**	**AP-P4+LC12**	**AP-P4**	**AP-P4+LC12**
Curve No	I	II	III	IV	V	VI
static adsorption (μg/g)	174.85 ± 11.35	102.06 ± 23.42	364.62 ± 17.63	139.80 ± 12.46	568.94 ± 11.87	242.91 ± 21.26

The curves of static adsorption of blank solution and polymer solution after the addition of stabilizer versus ageing time were obtained after linear fitting (Fig. 8), and the parameters of the fitted equations are shown in Table 9. The static adsorption amounts for both systems increased with extended aging time; however, the LC12 stabilized system consistently exhibited much lower adsorption. As detailed in Table 8, after 46 days, the static adsorption of the blank AP-P4 solution surged to 568.94 μg/g, whereas the AP-P4/LC12 system was restricted to 242.91 μg/g, representing a 57.3% reduction in chemical loss to the rock matrix.

Table 9: Parameters for fitting the curve of static adsorption and ageing time.

Samples	Fitted Curves y = a + bx	Correlation Coefficient R^2
AP-P4	y = 169.80205 + 11.9050x	0.99892
AP-P4+LC12	y = 90.6696 + 3.03945x	0.83984

Interestingly, experimental results indicated a decrease in the static adsorption capacity of the AP-P4/LC12 system compared to the pure AP-P4, yet a significant increase in the Resistance Factor (R_F) was observed during core flooding. This seemingly contradictory phenomenon can be attributed to the evolution

of the supramolecular structure. As a structural reinforcer, LC12 promotes the formation of larger and more robust hydrophobic aggregates through a 'nucleation and bridging' mechanism. Under static conditions, these large-sized aggregates reduce the effective specific surface area of the polymer chains, thereby decreasing the probability of interaction with active sites on the quartz sand surface, which manifests as lower adsorption. However, under dynamic flow conditions in porous media, these reinforced aggregates are more susceptible to mechanical trapping at pore throats. This physical entrapment contributes more significantly to flow resistance than simple surface adsorption, leading to a higher R_F. This suggests that the enhancement of mobility control by LC12 is a combined result of improved bulk viscosity and optimized retention mechanisms in the reservoir rock.

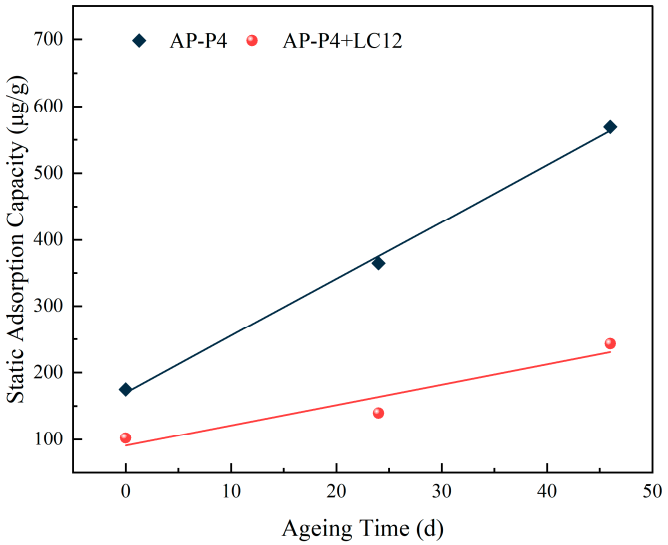

Figure 8: Static adsorption amount versus ageing time.

(5) Rheological properties

According to the experimental results on the rheology (Fig. 9) and viscoelasticity (Fig. 10) of the AP-P4 solution under different ageing times of the stabilizer, the solution viscosity, elastic modulus, and viscous modulus decreased with increasing ageing time before and after the addition of the stabilizer. Under the same ageing time, the addition of stabilizer LC12 increased the elastic modulus G′ of the polymer solution, which could significantly improve the elasticity of the polymer solution. Similarly, the addition of stabilizer LC12 increased the viscous modulus G″ of the polymer solution.

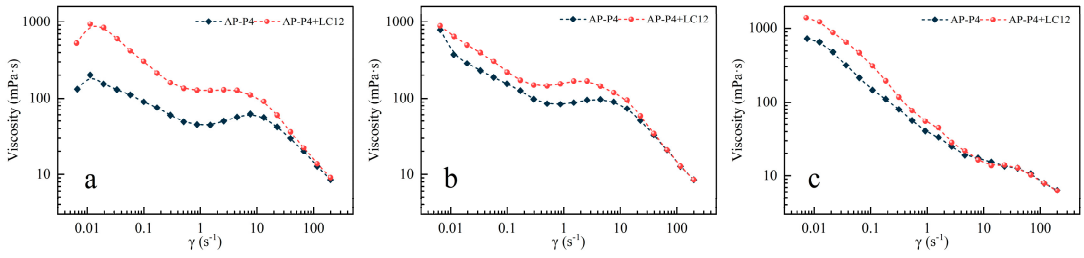

Figure 9: Influence of the stabilizer on the rheology of the AP-P4 solution ((**a**): ageing 0 d; (**b**): ageing 24 d; (**c**) ageing 46 d).

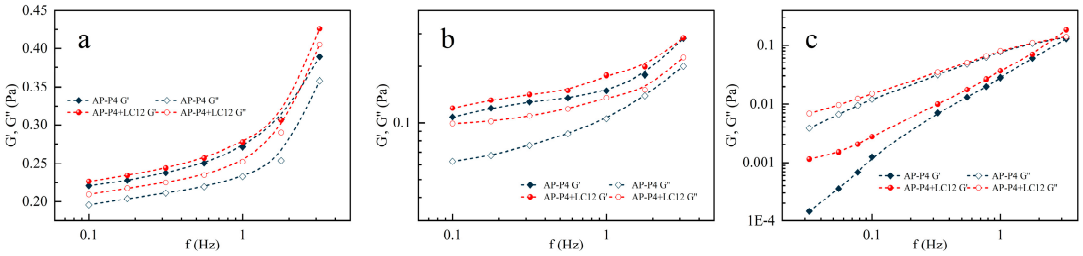

Figure 10: Influence of stabilizer on the viscoelasticity of AP-P4 solution ((**a**): ageing 0 d; (**b**): ageing 24 d; (**c**): ageing 46 d).

It is worth noting that while direct imaging of the microscopic aggregates remains a challenge, classic supramolecular network and transient gel theories provide a rigorous mathematical bridge between macroscopic viscoelasticity and microscopic network density. According to the classical affine network model, the plateau elastic modulus (G') of a physically cross-linked system is directly proportional to the number density of elastically active network chains or junction nodes per unit volume (ν), expressed as $G' \sim \nu k_B T$ (where k_B is the Boltzmann constant and T is the absolute temperature). In our dynamic oscillatory tests (Fig. 10), the multi-fold elevation of G' in the AP-P4/LC12 system compared to the blank matrix serves as a definitive thermodynamic indicator. It physically mandates a substantial increase in the density of active hydrophobic association nodes (ν). This macroscopic response mathematically validates the proposed 'nucleation and bridging' mechanism, proving that the strongly hydrophobic HAB segments of LC12 successfully act as aggregation nuclei that multiply the spatial physical cross-linking density.

(6) R_F and R_{RF}

The pressure profiles during the core flooding experiments are presented in Fig. 11. Based on the pressure data, the Resistance Factor (R_F) and Residual Resistance Factor (R_{RF}) were calculated using Eqs. (1) and (2), and the results are summarized in Table 10.

It was observed that both R_F and R_{RF} for the AP-P4 solution containing the LC12 stabilizer increased with aging time. A critical comparison between the static adsorption (Table 8) and the flow resistance data (Table 10) reveals an interesting phenomenon: although the static adsorption of the LC12-stabilized solution was lower than that of the blank AP-P4 solution, its Residual Resistance Factor (R_{RF}) was significantly higher.

This apparent contradiction can be explained by a shift in the retention mechanism. The blank AP-P4 solution primarily establishes residual resistance through adsorption on the rock surface. In contrast, the addition of LC12 promotes the formation of larger, more robust hydrophobic aggregates. While these larger aggregates have less specific surface area for adsorption (resulting in lower static adsorption), they are more prone to mechanical entrapment (plugging) within the pore throats of the core. This "log-jam" effect significantly enhances the flow resistance, thereby improving the mobility control capability of the polymer solution despite the reduced chemical loss to the rock.

(7) Injectivity and pore plugging assessment

Injectivity is a paramount parameter for evaluating the field applicability of EOR polymers, as excessive molecular aggregation may induce severe pore plugging and an uncontrollable rise in injection pressure. To assess the plugging risk of the AP-P4/LC12 system, the dynamic injection pressure was continuously recorded during the core flooding experiment (as illustrated in Fig. 11).

During the initial water flooding stage, the injection pressure remained low and stable at approximately 0.08 MPa. Upon switching to the AP-P4/LC12 polymer solution, the injection pressure exhibited a progressive

increase, which is primarily ascribed to the propagation of the high-viscosity fluid bank and the initial resistance established by the mechanical trapping of supramolecular aggregates at pore throats. Crucially, after the injection of approximately 7.63 PV, the pressure curve ceased to rise indefinitely and instead leveled off into a stable plateau at around 0.18 MPa. This stabilization indicates that a dynamic equilibrium between aggregate retention and hydrodynamic shearing was successfully established within the porous media. The absence of a continuous, linear upward trend in pressure strongly demonstrates that the AP-P4/LC12 system possesses excellent injectivity and poses negligible risk of irreversible, catastrophic formation plugging under reservoir conditions.

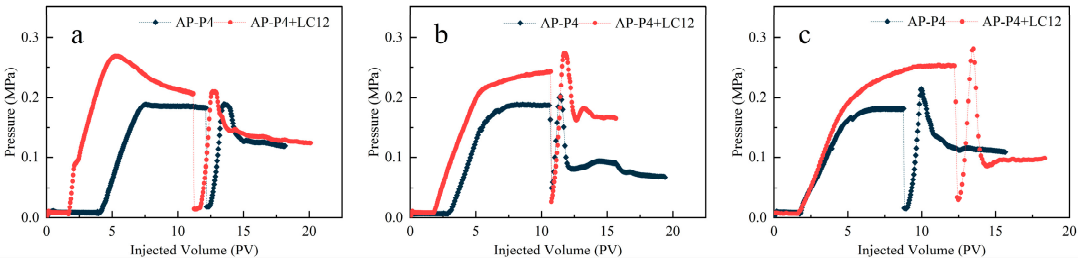

Figure 11: Influence of the stabilizer on the injection pressure of the AP-P4 solution ((**a**): ageing 0 d; (**b**): ageing 24 d; (**c**): ageing 46 d).

Table 10: Experimental results of R_F and R_{RF}.

Aging Time (d)	0		24		46	
Samples	**AP-P4**	**AP-P4+LC12**	**AP-P4**	**AP-P4+LC12**	**AP-P4**	**AP-P4+LC12**
ΔP_p (MPa)	0.1862	0.2088	0.1871	0.2402	0.1811	0.2522
ΔP_{wa} (MPa)	0.0083	0.0085	0.0066	0.0086	0.0084	0.0065
ΔP_{wb} (MPa)	0.1188	0.1242	0.0689	0.1654	0.1085	0.1295
R_F	22.4 ± 0.54	24.6 ± 0.85	28.3 ± 0.64	27.9 ± 0.75	21.5 ± 0.68	37.6 ± 0.71
R_{RF}	14.3 ± 0.73	14.6 ± 0.65	10.4 ± 0.68	19.2 ± 0.82	12.9 ± 0.76	19.9 ± 0.0.76

To profoundly understand the flow behavior of the AP-P4/LC12 system, it is imperative to view the dynamic retention through the lens of transport phenomena in porous media. As highlighted by the interfacial transport and confined-migration concepts recently elucidated by Zhao et al. [33], retention and flow resistance are not governed by isolated chemical mechanisms, but rather by the joint control of polymer–surface interactions and steric confinement.

In our static tests, the large robust aggregates formed by LC12 exhibited a reduced specific surface area, thereby weakening the pure chemical polymer–surface interaction and lowering static adsorption. However, during dynamic injection into the reservoir rock, these reinforced supramolecular aggregates encounter severe steric confinement within the tortuous pore throats. The transport mechanism fundamentally transitions from surface-dominated adsorption to confined-migration trapping. The physical dimensions of the LC12-bridged aggregates strategically mismatch with the pore-throat distributions, creating a highly effective mechanical “log-jam”. This steric entrapment profoundly amplifies the hydrodynamic flow resistance, leading to the significantly elevated R_F and R_{RF}.

Furthermore, this transport-based interpretation perfectly explains the excellent injectivity observed. After injecting approximately 7.63 PV, the injection pressure leveled off into a stable plateau at around 0.18 MPa. Rather than causing catastrophic irreversible plugging, the structurally reinforced aggregates achieve a dynamic confined-migration equilibrium: the rate of mechanical trapping at pore throats perfectly

balances with the hydrodynamic shearing and deformation of the dynamic physical networks. This ensures a highly stable displacement front, maximizing mobility regulation efficiency in deep formations.

(8) Oil flooding effect

Oil flooding experiments were conducted on polymer solutions with different ageing times after the addition of the stabilizer and compared with the oil flooding effect of polymer solutions without the stabilizer, and the results are shown in Fig. 12 and Table 11.

During the polymer injection phase (0.3 PV), the water cut exhibited a sharp decline (often referred to as a "kick-down" response), corresponding to a gradual increase in oil recovery. As shown in Table 11, the polymer solution stabilized with LC12 consistently yielded higher crude oil recovery compared to the blank solution across all aging intervals.

Notably, after 46 days of aging, the incremental oil recovery (the difference between polymer flooding recovery and water flooding recovery) for the LC12 system was 18.47%, whereas the blank system only achieved 13.98%. This represents a net improvement of 4.49 percentage points in EOR efficiency attributable to the stabilizer. This demonstrates that LC12 effectively mitigates viscosity loss and structural degradation, thereby sustaining the oil displacement efficiency of the polymer solution under reservoir conditions.

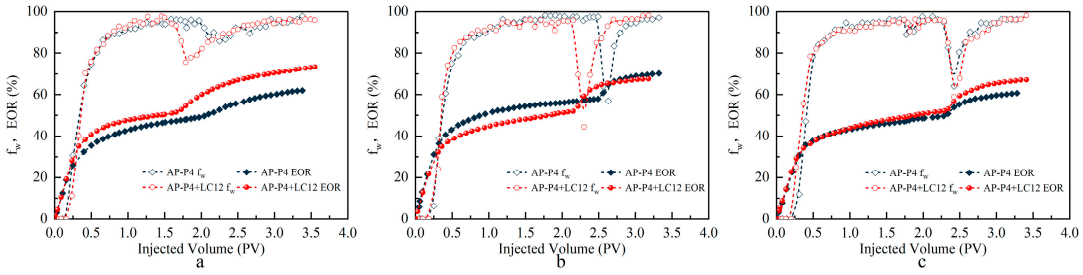

Figure 12: Influence of stabilizer on polymeric flooding water content and recovery ((**a**): ageing 0 d; (**b**): ageing 24 d; (**c**): ageing 46 d).

Table 11: Results of oil flooding experiments.

Aging Time (d)	0		24		46	
Samples	**AP-P4**	**AP-P4+LC12**	**AP-P4**	**AP-P4+LC12**	**AP-P4**	**AP-P4+LC12**
Permeability (mD)	2643	2431	1559	1746	2369	1998
Porosity (%)	30.29	30.30	30.31	27.45	29.90	30.30
Oil content saturation (%)	82.67	90.67	80.00	88.24	86.49	81.33
Water-flooding recovery (%)	46.33	47.65	55.44	46.08	47.87	45.87
Polymer-flooding recovery (%)	61.96	63.68	70.29	64.67	61.85	64.34
Incremental oil recovery (%)	15.63	16.03	14.85	18.59	13.98	18.47

3.3 Economic Feasibility and Scalability Analysis

To evaluate the potential for field application, the scalability and cost-effectiveness of LC12 were rigorously assessed. As recently highlighted by Chen et al. [34], the interplay between a polymer's processing design and its structural robustness is critical in determining both its macroscopic mechanical performance and ultimate economic feasibility. In alignment with this paradigm, our specific processing design—utilizing micellar polymerization to graft strongly hydrophobic HAB blocks—endows the LC12/AP-P4 system with exceptional structural robustness against severe mechanical shearing and thermo-oxidative degradation.

From a scalability perspective, the synthesis of the hydrophobic monomer HAB utilizes readily available industrial precursors (hexadecyl dimethylamine and 6-bromo-1-hexene) via a straightforward quaternization reaction with high yields (>90%). The subsequent preparation of LC12 is highly compatible with existing industrial production lines for polyacrylamide. Regarding economic feasibility, although the unit price of functional monomers like HAB is marginally higher than that of acrylamide, the optimal dosage of LC12 required to achieve this structural robustness is remarkably low (25 mg/L). Given the observed 4.49% increase in oil recovery over conventional polymer flooding, the return on investment (ROI) is highly favorable. This high efficiency-to-cost ratio, driven by rational processing design, strongly supports the large-scale deployment of LC12 as a practical EOR stabilizer in harsh reservoir environments.

4 Conclusions

In response to the severe shear and thermo-oxidative degradation that compromises polymer flooding efficiency in challenging reservoir environments, a novel polymeric viscosity stabilizer, LC12, was successfully developed via the micellar copolymerization of a tailored hydrophobic monomer (hexadecyldimethyl-5-enhexyl ammonium bromide) with acrylamide and sodium dodecyl sulfate. The incorporation of trace amounts of LC12 into the hydrophobically associating polymer (AP-P4) matrix not only accelerated the macroscopic dissolution rate but also significantly enhanced the viscoelastic properties of the fluid system before and after degradation. Mechanistically, the strongly hydrophobic blocks of LC12 act as association nuclei, physically reinforcing the supramolecular network through a robust “nucleation and bridging” effect. Interestingly, while the addition of LC12 effectively suppressed the static surface adsorption of the polymer onto rock surfaces, it promoted the formation of dense aggregates that shifted the primary retention mechanism in porous media toward mechanical trapping. This structural reinforcement and optimized pore-scale transport behavior translated to a 28.4% increase in shear viscosity retention and a substantial 4.49 percentage point improvement in incremental oil recovery compared to the unstabilized polymer. Ultimately, this study not only demonstrates the superior engineering feasibility of the LC12/AP-P4 system for deep reservoir mobility control, but also provides critical theoretical insights into the molecular design of high-performance chemical flooding formulations.

Acknowledgement: The authors acknowledge financial support from Sichuan Provincial Key Research and Development Program (Grant No. 2026YFHZ0249).

Funding Statement: This work was supported by the Sichuan Provincial Key Research and Development Program (Grant No. 2026YFHZ0249, awarded to Jie Cao).

Author Contributions: Yong Qi: Conceptualization, Investigation, Data Curation, Formal Analysis, Writing—Original Draft, Visualization. Jie Cao: Methodology, Validation, Writing—Review & Editing, Supervision, Project Administration. Wanfa Liu and Shiyuan Liu: Writing–Original Draft. All authors reviewed and approved the final version of the manuscript.

Availability of Data and Materials: The data that support the findings of this study are available from the Author Yong Qi, upon reasonable request.

Ethics Approval: Not applicable.

Conflicts of Interest: The authors declare no conflicts of interest.

References

1. Thomas S. Enhanced oil recovery—An overview. Oil Gas Sci Technol Rev IFP. 2007;63(1):9–19. [CrossRef].

2. Verma J, Mandal A. Potential effective criteria for selection of polymer in enhanced oil recovery. Petrol Sci Technol. 2022;40(7):879–92. [CrossRef].
3. Prakash S, Joshi D, Ojha K, Mandal A. Enhanced oil recovery using polymer alternating CO_2 gas injection: Mechanisms, efficiency, and environmental benefits. Energy Fuels. 2024;38(7):5676–89. [CrossRef].
4. Mandal A. Chemical flood enhanced oil recovery: A review. Int J Oil Gas Coal Technol. 2015;9(3):241. [CrossRef].
5. Wang X, Alvarado V, Marcy P, Wu X, Huzurbazar S. Global sensitivity analysis of CO_2 storage in fractured aquifers via computer experiments. Int J Greenh Gas Control. 2022;120:103760. [CrossRef].
6. Wang X, Liu W, Shi L, Zou Z, Ye Z, Wang H, et al. A comprehensive insight on the impact of individual ions on Engineered Waterflood: With already strongly water-wet sandstone. J Petrol Sci Eng. 2021;207:109153. [CrossRef].
7. Afolabi F, Mahmood SM, Yekeen N, Akbari S, Sharifigaliuk H. Polymeric surfactants for enhanced oil recovery: A review of recent progress. J Petrol Sci Eng. 2022;208:109358. [CrossRef].
8. Belhaj AF, Elraies KA, Mahmood SM, Zulkifli NN, Akbari S, Hussien OS. The effect of surfactant concentration, salinity, temperature, and pH on surfactant adsorption for chemical enhanced oil recovery: A review. J Petrol Explor Prod Technol. 2020;10(1):125–37. [CrossRef].
9. Gbadamosi A, Patil S, Kamal MS, Adewunmi AA, Yusuff AS, Agi A, et al. Application of polymers for chemical enhanced oil recovery: A review. Polymers. 2022;14(7):1433. [CrossRef].
10. Lu X, Cao B, Xie K, Cao W, Liu Y, Zhang Y, et al. Enhanced oil recovery mechanisms of polymer flooding in a heterogeneous oil reservoir. Petrol Explor Dev. 2021;48(1):169–78. [CrossRef].
11. Li Z, Hou J, Liu W, Liu Y. Multi-molecular mixed polymer flooding for heavy oil recovery. J Dispers Sci Technol. 2022;43(11):1700–8. [CrossRef].
12. Kakati A, Kumar G, Sangwai JS. Low salinity polymer flooding: Effect on polymer rheology, injectivity, retention, and oil recovery efficiency. Energy Fuels. 2020;34(5):5715–32. [CrossRef].
13. Mohsenatabar Firozjaii A, Zargar G, Kazemzadeh E. An investigation into polymer flooding in high temperature and high salinity oil reservoir using acrylamide based cationic co-polymer: Experimental and numerical simulation. J Petrol Explor Prod Technol. 2019;9(2):1485–94. [CrossRef].
14. Sircar A, Rayavarapu K, Bist N, Yadav K, Singh S. Applications of nanoparticles in enhanced oil recovery. Petrol Res. 2022;7(1):77–90. [CrossRef].
15. Zhao S, Zhu D, Bai B. Experimental study of degradable preformed particle gel (DPPG) as temporary plugging agent for carbonate reservoir matrix acidizing to improve oil recovery. J Petrol Sci Eng. 2021;205:108760. [CrossRef].
16. Davoodi S, Al-Shargabi M, Wood DA, Rukavishnikov VS, Minaev KM. Experimental and field applications of nanotechnology for enhanced oil recovery purposes: A review. Fuel. 2022;324:124669. [CrossRef].
17. Zhu S, Ye Z, Liu Z, Chen Z, Li J, Xiang Z. Adsorption characteristics of polymer solutions on media surfaces and their main influencing factors. Polymers. 2021;13(11):1774. [CrossRef].
18. Ferreira VHS, Moreno RBZL. Polyacrylamide mechanical degradation and stability in the presence of iron. In: Proceedings of the OTC Brasil; 2017 Oct 24–26; Rio de Janeiro, Brazil. [CrossRef].
19. Sandengen K, Meldahl MM, Gjersvold B, Molesworth P, Gaillard N, Braun O, et al. Long term stability of ATBS type polymers for enhanced oil recovery. J Petrol Sci Eng. 2018;169:532–45. [CrossRef].
20. Unsal E, ten Berge ABGM, Wever DAZ. Low salinity polymer flooding: Lower polymer retention and improved injectivity. J Petrol Sci Eng. 2018;163:671–82. [CrossRef].
21. Zhao Y, Yin S, Seright RS, Ning S, Zhang Y, Bai B. Enhancing heavy-oil-recovery efficiency by combining low-salinity-water and polymer flooding. SPE J. 2021;26(3):1535–51. [CrossRef].
22. Du J, Lv C, Lan X, Song J, Liu P, Chen X, et al. A review on viscosity retention of PAM solution for polymer flooding technology. Petrol Sci Technol. 2024;42(3):372–405. [CrossRef].
23. Ding X, Xu G, Liu WV, Yang L, Albijanic B. Effect of polymer stabilizers' viscosity on red sand structure strength and dust pollution resistance. Powder Technol. 2019;352:117–25. [CrossRef].
24. Groenendijk DJ, Bouts S, van Wunnik JNM. Performance improvement of chemical enhanced oil recovery by divalent ion–complexing agents. J Petrol Sci Eng. 2022;215:110609. [CrossRef].

25. Fu C, Huang K, Chen H, Huang B, Zhang W. From fundamental mechanisms to applications and challenges of nanofluid flooding in enhanced oil recovery: A review. Fuel. 2025;396:135317. [CrossRef].
26. Kakati A, Bera A, Al-Yaseri A. A review on advanced nanoparticle-induced polymer flooding for enhanced oil recovery. Chem Eng Sci. 2022;262:117994. [CrossRef].
27. Kang W, Sarsenbekuly B, Turtabayev S, Yang H, Zhu T, Aidarova S, et al. Study on the influence of emulsification property of functional polymers on enhanced oil recovery and its mechanism. J Petrol Sci Eng. 2020;185:106627. [CrossRef].
28. Kesarwani H, Sharma S, Mandal A. Application of novel colloidal silica nanoparticles in the reduction of adsorption of surfactant and improvement of oil recovery using surfactant polymer flooding. ACS Omega. 2021;6(17):11327–39. [CrossRef].
29. Shi L, Zhu S, Guo Z, Zhao W, Xue X, Wang X, et al. Experimental study on the effect of polymer injection timing on oil displacement in porous media. Processes. 2020;8(1):93. [CrossRef].
30. Mao J, Tan H, Yang B, Zhang W, Yang X, Zhang Y, et al. Novel hydrophobic associating polymer with good salt tolerance. Polymers. 2018;10(8):849. [CrossRef].
31. Patel V, Sharma T. On the rheology and polymer conformation of associative polymers. Polym Bull. 2023;80:8939–59.
32. Deng H, Yang Z, Zhou M, Ou E, Lu Y, Zhou Q, et al. Anionic polymerization of (Z)-1, 3-pentadiene using Ba/Al/Li trimetallic initiators to synthesize crystalline high trans-1, 4-polypentadiene. Polymer. 2024;315:127841. [CrossRef].
33. Zhao G, Gao H, Qu Z, Fan H, Meng H. Anhydrous interfacial polymerization of sub-1 Å sieving polyamide membrane. Nat Commun. 2023;14:7624. [CrossRef].
34. Chen B, Wang C, Zhang L, Wang C. Synthesis of starch-based polyether non-isocyanate polyurethane with excellent mechanical and foaming properties. Int J Biol Macromol. 2025;330:148147. [CrossRef].